

Comparison of traveltimes inversions on a limestone structure

Matthew D. Allen and Robert R. Stewart

ABSTRACT

Four traveltimes inversion techniques were applied to two sets of seismic data collected on a Maya pyramid ruin at Maax Na, Belize. In particular, direct division, singular value decomposition, damped least squares and the conjugate gradient methods were applied. The seismic data consists of two source-receiver rings around the circumference of the pyramid with one ring near the base, and the other near the top of the pyramid. All methods produced similar velocity fields with most velocities in the range of 200-800m/s (characteristic of carbonate rubble).

Traveltimes residuals (observed minus calculated times) show an average of approximately 3ms for each method. However, based on the average and standard deviation of the residuals, the most accurate technique was found to be direct division followed by damped least-squares, singular value decomposition and lastly conjugate gradient.

INTRODUCTION

Seismic tomography is starting to be applied to the field of archaeology (Merlanti and Musante 1994; Cardarelli and de Nardis 2001; Karastathis et al. 2001; Aitken and Stewart, 2003). Archaeological practices generally concentrate on excavations of a small scale as they are costly, time consuming and invasive. When considering a large area such as an ancient city it would be an immense effort to excavate the whole area. To ameliorate this problem, geophysical practices are being considered as relatively inexpensive, rapid and non-invasive techniques. By using geophysics, archaeologists might be directed to ideal locations to excavate. In some cases, the geophysical techniques can be used to determine whether structures should be excavated or left untouched.

One such area where geophysical practices are being used to help archaeology was in Maax Na, Belize. In the summer of 2002, seismic imaging was used on the large pyramid at Maax Na. The pyramid is approximately 28m by 28m and stands around 15m high as seen in Figure 1. The seismic data was acquired using sixty-one hammer seismic sources with sixty 1-component geophones, planted vertically, spread around the circumference of the pyramid. Hammer seismic has been shown to be an effective method for image acquisition on Maya pyramid ruins (Xu and Stewart 2000; 2001). However, to further develop seismic imaging to assist archaeological studies the data was used to determine the best analysis techniques for seismic imaging around pyramid ruins.

Two separate surveys were taken at Maax Na. The first survey was performed on the lower section of the pyramid. This survey had a horizontal receiver spacing of 2m and were spread along a contour level near the base of the pyramid. The shots were placed along the same vertical contour space in-between the receivers. As the circumference of the pyramid was not large enough to accommodate all of the receivers the final 4 receivers were placed perpendicular to the circumference and placed going down the

pyramid (Figure 2a). The second survey was performed further up the pyramid. The horizontal receiver spacing used was reduced to 1m with the hammer-sources once again being placed between the receivers. In this survey, there were not adequate receivers to cover the entire circumference therefore a gap in the coverage was left along the eastern side of the pyramid as seen in Figure 2b.

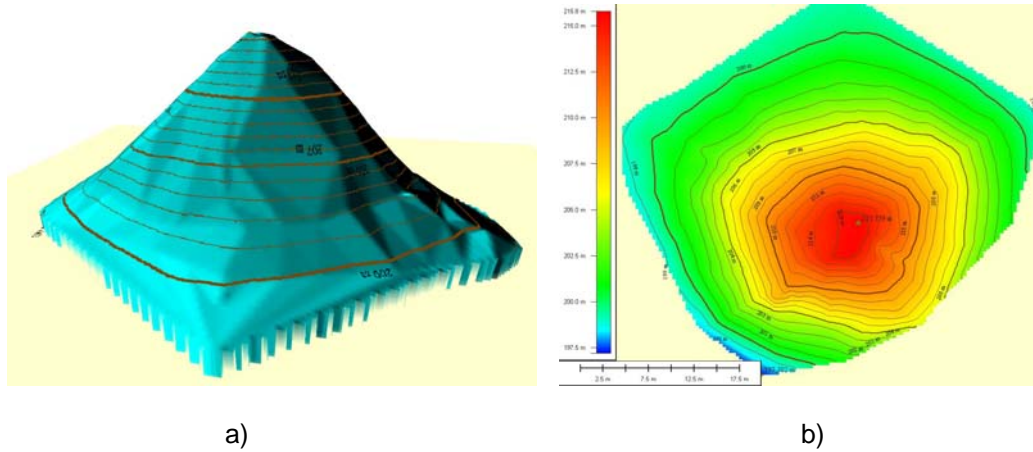
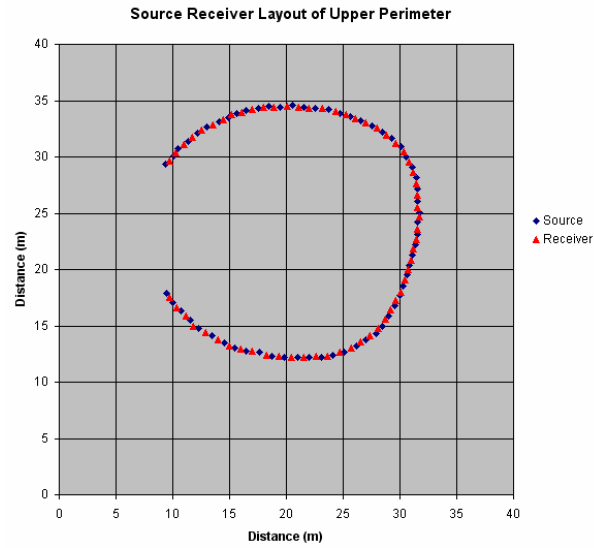
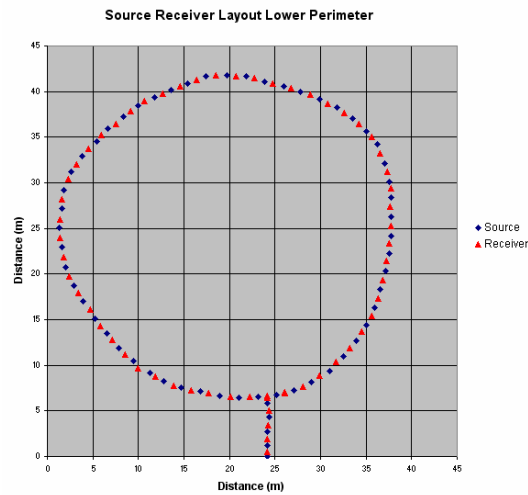


FIG. 1. A topographic map of the Maax Na pyramid shown in a) 3-D perspective and b) contour plan view.



a)



b)

FIG. 2. The source and receiver layout for the a) upper and b) lower perimeter of the Maax Na pyramid. Sources are indicated in blue and receivers are indicated in red.

DATA ANALYSIS

A seismic shot gather is considered “good”, if it has clear events and consistent first breaks. To better pick some of the more difficult first breaks, a 500ms AGC was applied to the trace. This often makes the first break clearer. A sample gather from the lower perimeter showing a single shot with first break picks is shown in Figure 3. In both the upper and lower perimeter data, there were a total of 61 shots and 60 receivers. This amounts to a total of 3660 traveltimes per survey.

Before processing the traveltimes an examination of the seismic gathers is undertaken. In assessing the lower surveys sections (See Figure 3) channel 1 and channel 35 appear to

be dead traces. These receivers were killed. During acquisition four source positions had to be abandoned due to an angry wasps nest. Finally, since we are using 2D traveltime inversion further exclusion of sources and receivers must be made. In order to perform an accurate inversion all locations must be on the same vertical contour. However, since there were extra sources and receivers some were placed further down the pyramid than the others. These shots can be re-included if 3D inversion techniques are applied. After the exclusion of these sources and receivers there will be a total of nine shots and six receivers being excluded. Taking this information into account the lower perimeter is left with 54 receivers and 52 shots resulting in 2808 traveltimes instead of the original 3660.

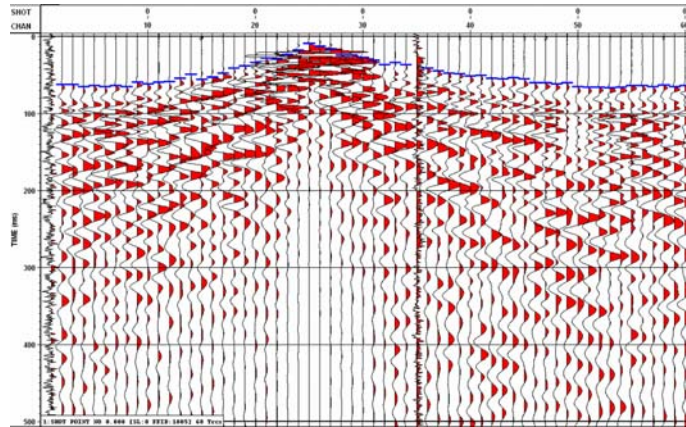


FIG. 3. A sample shot from the lower perimeter with a 500ms AGC. First break picks are shown in blue. Receivers 1 and 35 are dead.

The upper perimeter experienced difficulties as well. Due to a looter's trench that was dug out of the pyramid through the open gap in the survey (Figure 4), many rays had to be rejected. Since many rays passed through the empty trench they would result in many transmission effects that will alter the correct velocity structure of the pyramid. In order to compensate for this trench all rays passing through the trench were ignored. This brings the ray total from 3660 down to a total of 3054.

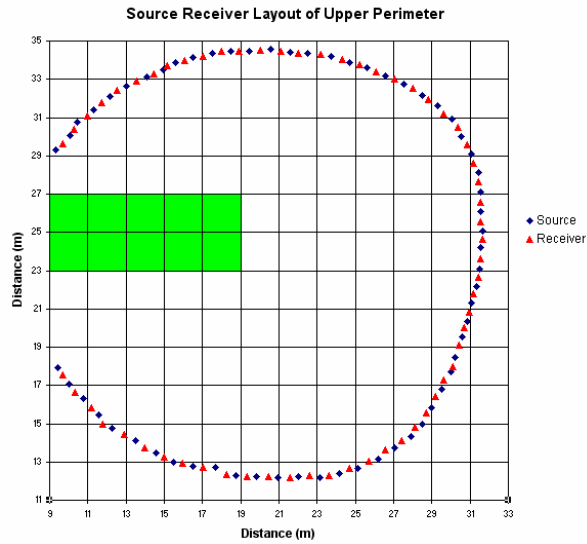


FIG. 4. The source receiver layout of the upper perimeter line with the approximate location of the looter’s trench in green.

The hammer-seismic source produced on average a relatively broadband signal up to 200Hz. However, some shots produced signal up to 300 Hz. These variations can be associated with differences in hammer speed and power. Figure 5 shows the FK spectrum of the shot from position 1. The remaining shots display similar results.

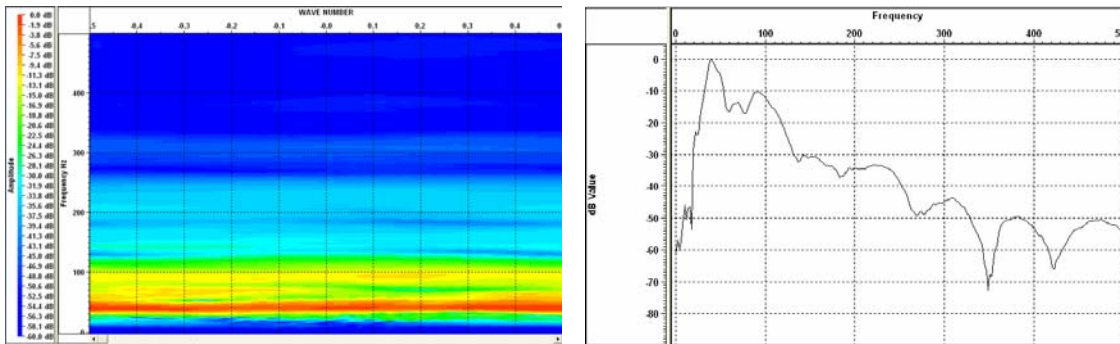


FIG. 5. The FK spectrum (left) and the amplitude spectrum for the average data trace of shot 1023.

A mathematical expression for the measure of error in the measurement of arrival time of the first motion is given by Stewart (1984) as

$$\Delta t = \frac{1}{f_m \log_2 \left(1 + \frac{S^2}{N^2} \right)}, \tag{1}$$

where f_m is the frequency of the arrival and S/N is the signal-to-noise ratio. As seen in Figure 5 the peak frequency is 40 Hz. This frequency was used as the frequency of the arrival. An estimated signal-to-noise ratio of 5.26 was found by dividing the RMS of the

peak arrival amplitude by the RMS of the peak noise amplitude. Solving equation (1) using these numbers a travelttime error of 4.8ms was found.

INVERSION

The four methods of inversion applied to the data were direct division, damped least-squares, singular value decomposition and conjugate gradient. All four methods are based on ray tracing techniques. Assuming straight ray paths the travelttime inversion is cast as a series of linear equations

$$T_i = \sum_j A_{ij} \cdot P_j \quad (2)$$

where T_i is the total travelttime of i^{th} shot-receiver pair, A_{ij} is the distance of the i^{th} ray through the j^{th} pixel and P_j is the slowness of the j^{th} pixel. Expressed in matrix form

$$T = AP \quad (3)$$

This is the equation used for direct division. However, the goal is to find the slowness value so to get the final direct division solution equation (3) must be modified to give

$$P = \frac{T}{A^T} \quad (4)$$

The damped least-squares solution is seen as an improvement on direct division in the case of inadequate or noisy data. The solution for damped least-squares is given by

$$P = (A^T A + \lambda^2 I)^{-1} A^T T \quad (5)$$

where λ is the damping factor. The damping factor used for the pyramid ruin data is 1e-06.

Singular value decomposition (SVD) was also developed as an improvement on direct division. Singular value decomposition breaks up the distance matrix to give

$$P = VL^{-1}U^T T \quad (6)$$

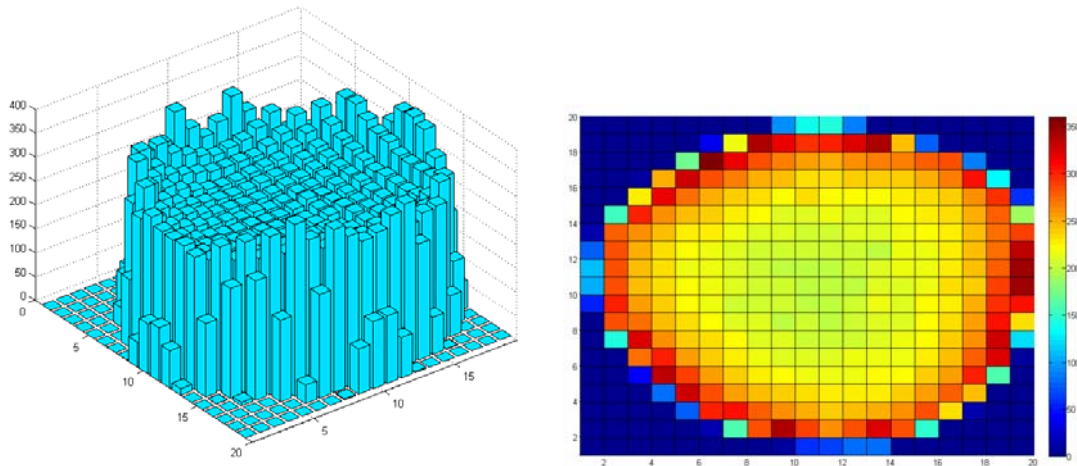
where the columns of U are equivalent to the eigenvectors of AA^T and the columns of V are the eigenvectors of $A^T A$ and L contains the non singular values of A .

The last technique used was the conjugate gradient method. The conjugate gradient method is a recursive method that works by minimizing a residual vector. After each iteration a more accurate velocity parameter is produced. A constraint of 30 iterations was placed for work on the pyramid data. Further description of the inversion techniques can be found in the appendix.

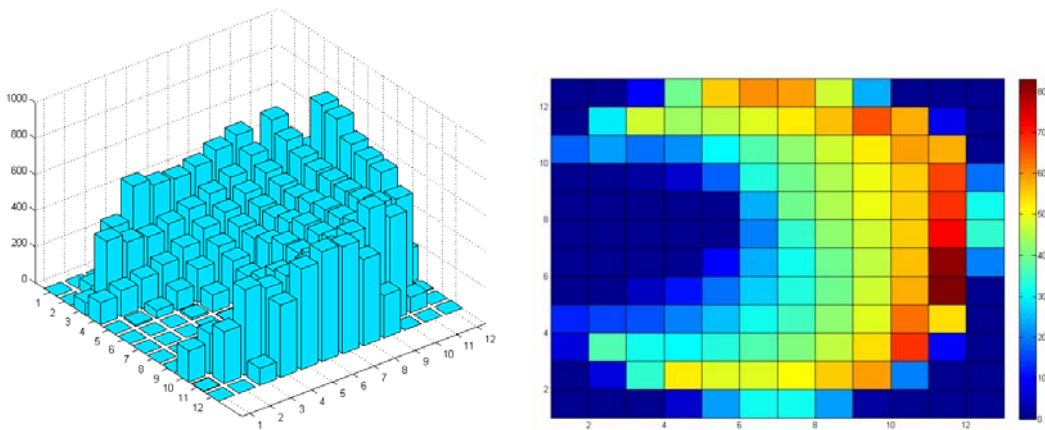
RAY TRACING

For the ray tracing a grid system of 2m by 2m pixels was found to give a high fold, see Figure 6, while remaining small enough to give a good picture of the velocity structure. For the lower circumference survey a grid system of 19 by 19 pixels was used. For the

upper survey a layout of 12 by 12 pixels were used. This results in an \mathbf{A} matrix of 2808x361 for the lower and 3054x144 for the upper survey.



a)



b)

FIG. 6. Total coverage of rays per pixel for a) lower and b) upper survey. Perspective and plane views of the coverage are shown. The x and y axes are the horizontal dimension of the survey and are given in meters.

RESULTS

Four different techniques were used to find the velocity structure of the pyramid including direct division, damped least-squares, singular value decomposition and conjugate gradient. All four techniques produced similar results for the lower survey with velocities in the range of 200-800m/s. Figure 7 shows the velocity structure of the lower survey found using SVD.

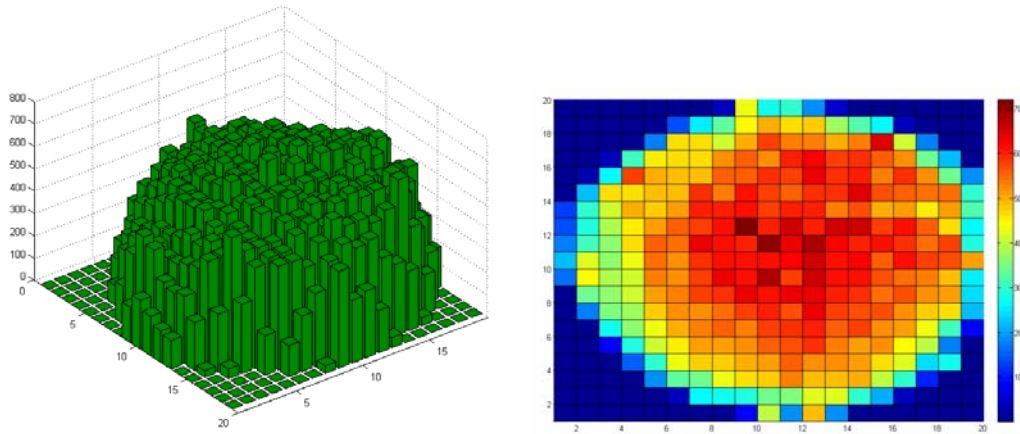


FIG. 7. The final velocity (m/s) map of the Maax Na pyramid found using singular value decomposition.

Solving for the velocity of the upper circumference multiple negative velocities were derived. These are clearly not physical therefore were set equal to zero for display purposes. All the negative values appeared in areas of low fold making them unreliable. While most of the techniques produced very similar results for the upper perimeter several high unphysical values were derived from the conjugate gradient method. These values can be seen in Figure 8. Once again these high values are in areas of lower fold resulting in values that are unreliable.

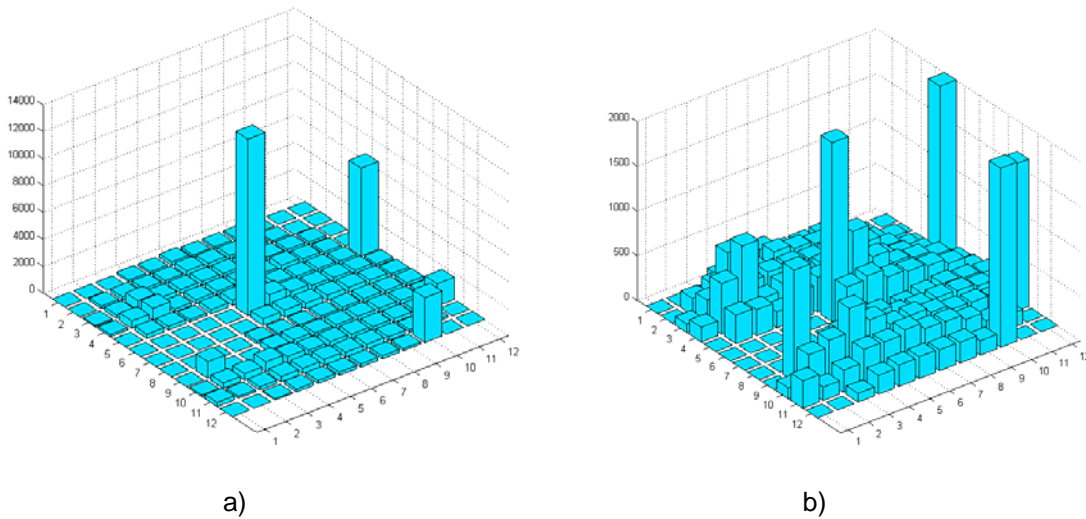


FIG. 8. The final conjugate gradient velocity (m/s) map of the Maax Na pyramid for the upper survey with a) no filtering and b) all velocities greater than 2000 set equal to 2000.

These conjugate gradient results can be compared to the similar velocity structures given by the other three methods. Figure 9 shows the velocity map derived from the SVD method that is very similar to the damped least squares and the direct division maps.

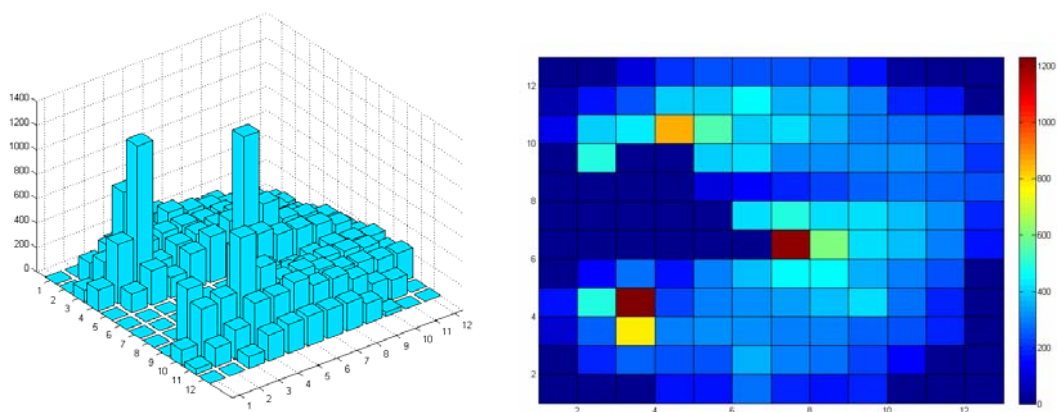


FIG. 9. The final velocity (m/s) map of the upper perimeter survey as derived from singular value decomposition.

A view of both the upper and lower velocity maps in relation to one another can be seen in Figure 10.

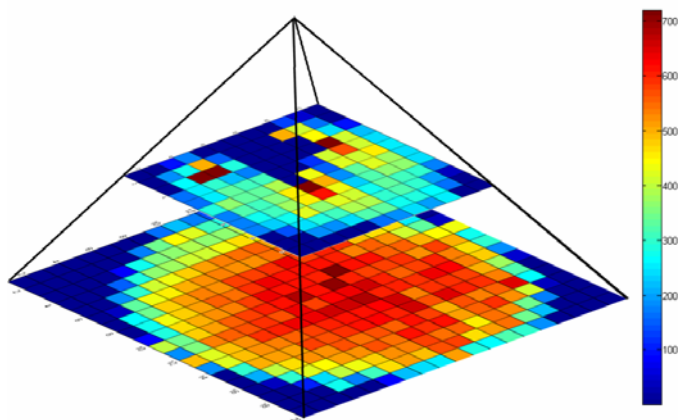


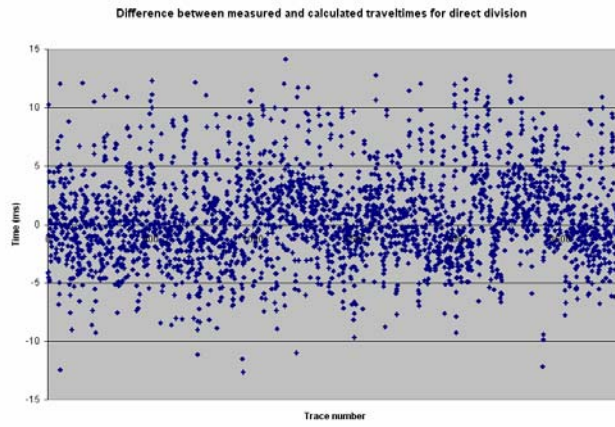
FIG. 10. The velocity (m/s) map of both the upper and lower surveys derived by SVD. The upper survey has been filtered so all velocities over 700 m/s are equal to 700 m/s.

COMPARISON

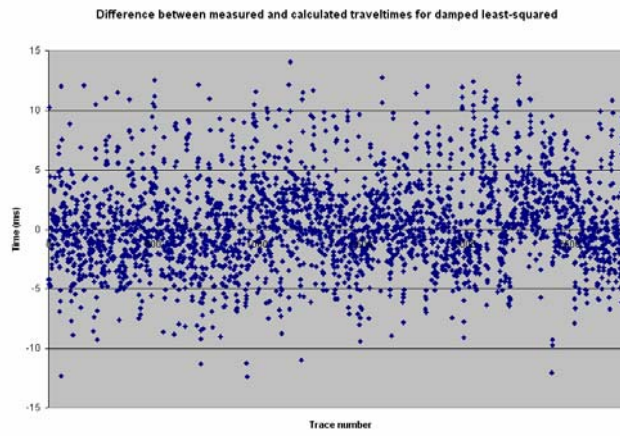
Using the velocity structures derived by the four different techniques and the distance matrix \mathbf{A} a set of traveltimes were found. These traveltimes were compared to the original traveltimes measured from the raw seismic.

Lower Perimeter

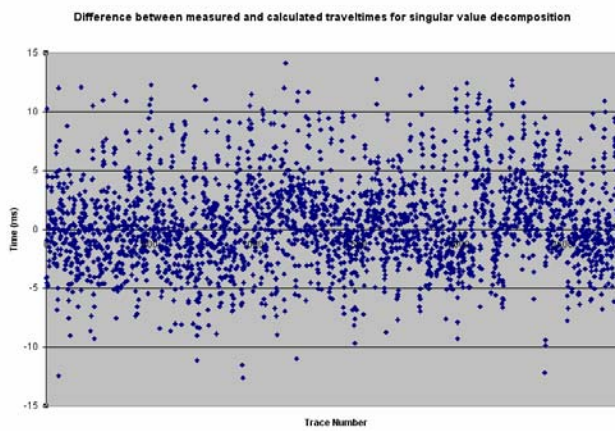
The differences between the measured and calculated were graphed and can be seen in Figure 11.



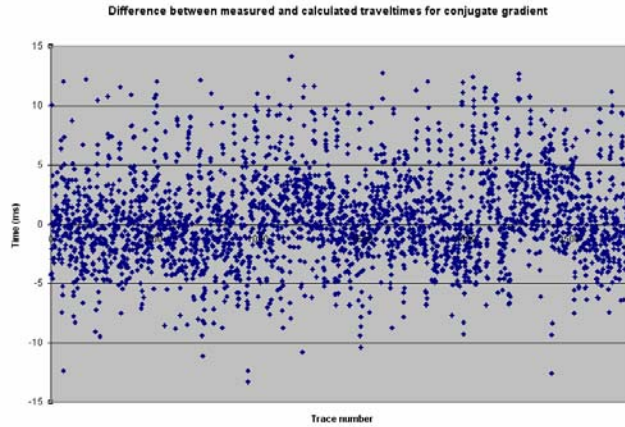
a)



b)



c)



d)

FIG. 11. The difference between measured and calculated lower perimeter traveltimes (ms) for a) direct division, b) damped least-squares, c) singular value decomposition and d) conjugate gradient.

The differences for each method are very similar. Most of the differences appear to be within 5ms of the measured traveltimes. However there are a few cases where the differences are around the 15ms range. These traveltimes are typically from pixels of low fold and therefore the velocity structure will not be as accurate resulting in erroneous traveltimes.

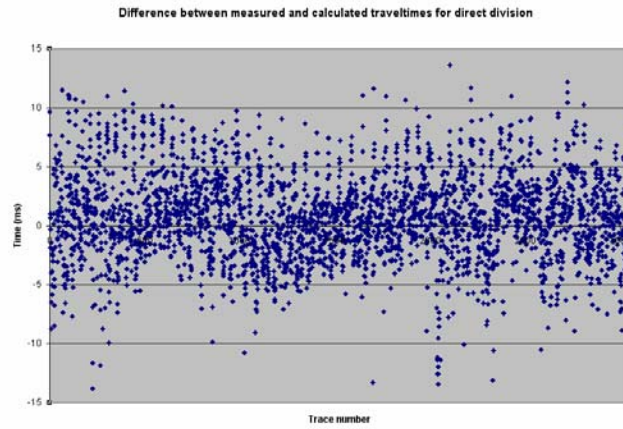
To determine the most accurate technique an average of the absolute value of the differences as well as the standard deviation of the differences was taken for each method as seen in Table 1.

Table 1. The average of the absolute value of the differences and the standard deviation values for all techniques on the lower perimeter.

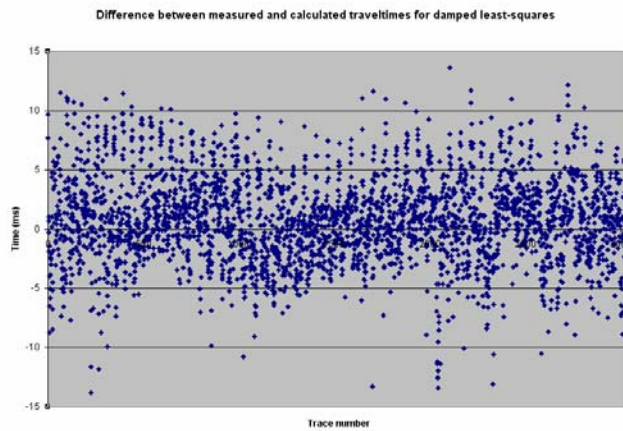
	Direct Division	Damped Least-squares	Singular Value Decomposition	Conjugate Gradient
Average	2.911	2.913	2.919	2.959
Standard Deviation	3.798	3.801	3.804	3.842

Upper Perimeter

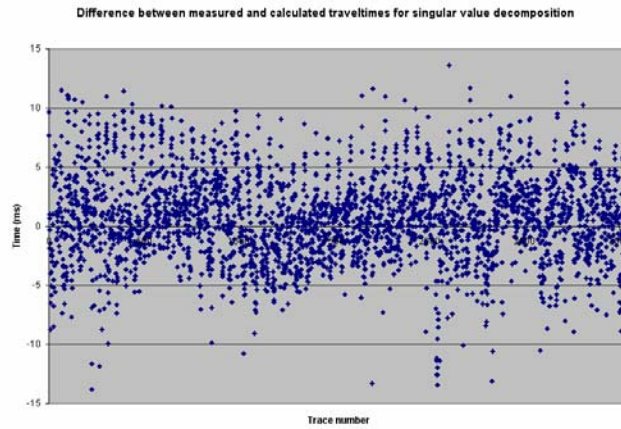
The differences between the measured and calculated traveltimes for the upper perimeter survey can be seen in Figure 12.



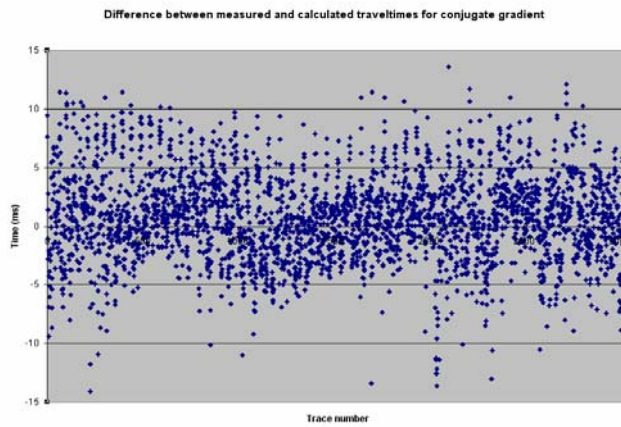
a)



b)



c)



d)

FIG. 12. The difference between measured and calculated upper perimeter traveltimes (ms) for a) direct division, b) damped least-squares, c) singular value decomposition and d) conjugate gradient.

Similar to the lower survey the different techniques are resulting in very similar differences. For all four techniques the majority of the differences are within the 5ms range indicating a fairly accurate velocity map. However there are larger differences up to approximately 14ms. Upon inspection of the large difference values the majority are found to be in these areas of low fold meaning the velocity structure of the region is not as accurate resulting in large traveltimes differences.

Since the differences between the four methods are so similar it is hard to determine which method is the most accurate. To get a better indication the average and standard deviation of the differences were once again taken to help get a determination. These values can be seen in Table 2.

Table 2. The average of the absolute value of the differences and the standard deviation values for all techniques on the upper perimeter.

	Direct Division	Damped Least-squares	Singular Value Decomposition	Conjugate Gradient
Average	2.890	2.890	2.892	2.911
Standard Deviation	3.665	3.665	3.667	3.682

CONCLUSIONS

Four different traveltimes inversion techniques were used on two different surveys from the Maax Na pyramid in Belize. All four methods produced velocity maps similar to those seen in Figure 7 for the lower survey and Figure 9 for the upper survey. Upon comparison with the first break traveltimes measured from the raw data we see that all four methods are very similar but there are differences. The most accurate method appears to be direct division followed by damped least-squares, singular value decomposition and finally conjugate gradient.

Direct division is perhaps the most accurate due to the scale and coverage of the surveys. Since we are dealing in a small scale (28m by 28m) there would be limited noise in the data. Also due to the almost 360 degree coverage we have good fold over most pixels there is adequate coverage for direct division to be accurate.

While the velocity structure appears good there is still an average of approximately 3ms difference between our calculated and measured traveltimes. This average is inside the estimated 4.8ms error for first break traveltimes. In order to improve on these results a curved ray as opposed to a straight ray tracer should be employed.

FUTURE WORK

In the future, we would like to solve this data set using different methods including finite difference traveltimes and 2d curved ray tracing. This data set can also be expanded into 3D. Along with the 2 perimeter surveys discussed in this paper multiple lines were shot vertically up the pyramid. Using all the available seismic lines a comparison of different techniques can be undertaken in 3D.

REFERENCES

- Aitken, J. and Stewart, R.R., 2003, Ground-Penetrating Radar (GPR) imaging of near- surface structure in a carbonate environment: CREWES Research Report, **15**.
- Cardarelli, E., de Nardis, R., 2001, Seismic refraction, isotropic anisotropic seismic tomography on an ancient monument (Antonino and Faustina temple AD 141): Geophysical Prospecting, **49**, 228-240.
- Karastathis, V.K., Papamarinopoulos, S., and Jones, R.E., 2001, 2-D velocity structure of the buried ancient canal of Xerxes: an application of seismic methods in archaeology: Journal of Applied Geophysics, **47**, 29-43.
- Lines, L.R., and Treitel, S., 1984, Tutorial a review of least-squares inversion and its application to geophysical problems: Geophysical Prospecting, **32**, 159-186.

- Mahmoudian, F., 2006, Linear AVO inversion of multi-component surface seismic and VSP data: M.Sc. Thesis, University of Calgary.
- Merlanti, F., and Musante, B., 1994, Seismic tomography: application for archaeological purposes: *Geoarchaeology*, **9**, 317-329.
- Michelena, R. J., 1993, Singular value decomposition for cross-well tomography: *Geophysics*, **58**, 1655-1661.
- Stewart, R. R., 1984, Vertical-seismic-profile (VSP) interval velocities from traveltimes inversion: *Geophysical Prospecting*, **32**, 608–628.
- Stewart, R.R., 1991, *Exploration Seismic Tomography: Fundamentals*, SEG Course Notes Series, **3**.
- Xu, C. and Stewart R.R., 2000, Seismic tomography of a Maya pyramid: Chan Chich, Belize: CREWES Research Report, **12**, 563-575.
- Xu, C. and Stewart R.R., 2001, Seismic tomography of a Maya pyramid ruin, Chan Chich, Belize: CREWES Research Report, **13**, 843-850.
- Yilmaz, O., 2001, *Seismic data analysis: processing, inversion and interpretation of seismic data*. Vol 2. Society of Exploration Geophysicists, 1528-1530.

APPENDIX

Direct Division

To find the velocity structure inside the temple we must use an inversion technique. In this case we use a series expansion method. This method involves dividing the area of interest, in this case the pyramid, into pixels. From here we can use ray tracing through the pixels to find a sum of the pixel values (Stewart, 1991). The pixels can be defined to have a length l and a height h . The distance that the ray travels through a pixel can be given by d where D gives the total length of the ray as seen in Figure 5. Finally we set the slowness to be equal to p .

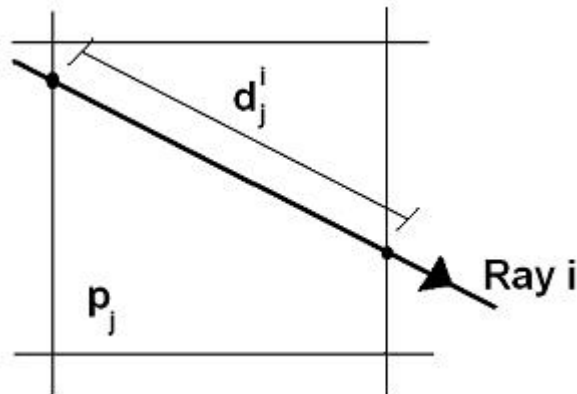


FIG. A-1. A ray propagating through a single pixel where d_j^i is the distance that ray i travels in pixel j and p_j is the slowness of pixel j and the traveltimes is given by $t=dp$, (Stewart, 1991)

Since we know the travel times of the rays we want a formula that incorporates both the travel time, which we know, and the velocity or slowness, which we want to find. We can find the travel time of a ray traveling through a single pixel to be equal to

$$t = dp . \tag{A-1}$$

Using the equation for the travel time through a single pixel we can find the equation for the travel time through all the pixels. This can be expressed as for the first given ray as,

$$t^1 = d_1^1 p_1 + d_2^1 p_2 + d_3^1 p_3 + \dots + d_M^1 p_M, \quad (\text{A-2})$$

$$= \sum_{j=i}^M d_j^1 p_j \quad (\text{A-3})$$

where M is the number of pixels in the object, j is the pixel number, and i is the ray number. (Stewart, 1991) Each shot receiver pair makes up one equation giving us a system of linear equations. Expressing this equation in matrix form we get

$$T = AP \quad (\text{A-4})$$

where T is the traveltimes vector, A is the raypath geometry matrix and P is the slowness vector.

Using this equation we can find the traveltimes of the rays given the slowness values and the ray path. However, since we have the traveltimes and are looking for the slowness values we must solve the inverse problem. The exact solution for this inverse problem is given by

$$P = A^{-1}T. \quad (\text{A-5})$$

In order to solve for the slowness using matrix values equation (A-5) was modified to the direct division equation given by

$$P = \frac{T}{A^T}. \quad (\text{A-6})$$

Damped Least Squares

In the presence of noise or inadequate observations the least squares solution is seen as an improvement on direct division. The least-squares solution (Lines and Treitel, 1984) is given by

$$P = (A^T A)^{-1} A^T T. \quad (\text{A-7})$$

In order to obtain more stability in the solution a damping term may be added. This results in the damped least squares equation

$$P = (A^T A + \lambda^2 I)^{-1} A^T T, \quad (\text{A-8})$$

where λ^2 is the damping parameter and I is the identity matrix.

Singular Value Decomposition

The benefit of singular value decomposition (SVD) is that it provides a precise way of analyzing a matrix, which results in a stable and approximate inverse (Mahmoudian, 2006). The SVD method allows the matrix to be expressed as the product of three matrices,

$$A = ULV^T, \quad (A-9)$$

where \mathbf{U} is an $m \times m$ orthonormal matrix of eigenvectors that span the data space, \mathbf{V} is an $n \times n$ orthonormal matrix that spans the model space and \mathbf{L} is the $m \times n$ matrix that contains the non-zero singular values of \mathbf{A} in its diagonal elements (Michelena, 1993). The columns of \mathbf{U} are equivalent to the eigenvectors of $\mathbf{A}\mathbf{A}^T$ and the columns of \mathbf{V} are the eigenvectors of $\mathbf{A}^T\mathbf{A}$. Inserting the SVD of matrix \mathbf{A} into equation A-5 the equation for the slowness is given by

$$P = VL^{-1}U^T T, \quad (A-10)$$

There are a few advantages of the SVD method over the least squares method. The main advantage comes when dealing with a matrix that is singular or near singular. The SVD will still work with these matrices and can produce a numerical answer that is stable (Mahmoudian, 2006).

Conjugate Gradient

The conjugate gradient method starts with the least squares solution of equation (A-7). This equation can be arranged to by the normal equation given by

$$A^T A P = A^T T. \quad (A-11)$$

Following the method described in Yilmaz (2001) \mathbf{D} is defined by

$$D = A^T A, \quad (A-12)$$

and \mathbf{B} is defined as

$$B = A^T T, \quad (A-13)$$

resulting in

$$DP = B. \quad (A-14)$$

In order to recursively find an estimated value for \mathbf{P} we start with an initial estimate \mathbf{X}_0 . This initial estimate can be defined as a null vector and is terminated when the residual vector \mathbf{R}_i defined by

$$R_i = B - DX_i \quad (A-15)$$

becomes a null vector. Where \mathbf{X}_i is the parameter vector estimate after the i th iteration and if the matrix \mathbf{D} has dimensions $n \times n$ the conjugate gradient method will yield the solution after $m < n$ iterations.

The initial values used in the conjugate gradient method are given by

$$c_{-1} = 1, \quad (A-16)$$

$$G_{-1} = 0, \quad (A-17)$$

and

$$R_0 = B - DX_0. \quad (\text{A-18})$$

To start the recursion, first compute the initial residual error c_0 using

$$c_i = R_i^T R_i, i = 0, 1, 2, \dots, m, \quad (\text{A-19})$$

where c_i is the residual energy after the i^{th} iteration. Input the derived value of c_0 and the value of c_{-1} given in equation 16 to the formula

$$b_{i-1} = \frac{c_i}{c_{i-1}}, \quad (\text{A-20})$$

using the derived value of b_{-1} and the values of \mathbf{G}_{-1} (equation A-16) and \mathbf{R}_0 (equation A-17) in the equation

$$G_i = R_i + b_{i-1}G_{i-1} \quad (\text{A-21})$$

a value of \mathbf{G}_0 can be obtained.

Applying the equations:

$$Q_i = DG_i, m \leq n, \quad (\text{A-22})$$

$$d_i = G_i^T Q_i, \quad (\text{A-23})$$

$$a_i = \frac{c_i}{d_i}, \quad (\text{A-24})$$

and

$$X_{i+1} = X_i + a_i G_i \quad (\text{A-25})$$

a value for the parameter vector estimate \mathbf{X}_1 can be derived. Finally the new residual vector \mathbf{R}_1 is given by

$$R_{i+1} = R_i - a_i Q_i \quad (\text{A-26})$$

Plug the value of \mathbf{R}_1 back into equation A-19 and repeat the calculations of equation A-18 through equation A-26. This could be done for any specified number of iterations where $m < n$.